Chapter 3

Scale Dependence of the Thermodynamic Forcing of Tropical Monsoon Clouds: Results from TRMM Observations

Abstract

Clouds exert a thermodynamic forcing on the ocean-atmosphere column through latent heating, owing to the production of rain, and cloud radiative forcing, owing to the absorption of terrestrial infrared energy and the reflection of solar energy. The Tropical Rainfall Measuring Mission (TRMM) satellite provides, for the first time, simultaneous measurements of each of these processes on the spatial scales of individual clouds. Data from TRMM are used to examine the scale dependence of the cloud thermodynamic forcing and to understand the dominant spatial scales of forcing in monsoonal cloud systems. The tropical Indian Ocean is chosen, because the major monsoonal cloud systems are located over this region. Using threshold criteria, the satellite data are segmented into rain cells (consisting of only precipitating pixels) and clouds (consisting of precipitating as well as nonprecipitating pixels), ranging in scales from 10^3 km^2 to 10^6 km^2. For each rain cell and cloud, latent heating is estimated from the microwave imager and radiative forcing is estimated from the Clouds and the Earth's Radiant Energy System radiation budget instrument.

The sizes of clouds and rain cells over the tropical Indian Ocean are distributed lognormally. Thermodynamic forcing of clouds increases with rain cell and cloud area. For example, latent heating increases from about 100 W m^{-2} for a rain cell of 10^3 km^2 to as high as 1500 W m^{-2} for a rain cell of 10^6 km^2. Correspondingly, the liquid water path increases tenfold from 0.3 kg m^{-2} to nearly 3 kg m^{-2}, the longwave cloud forcing from 30 to 100 W

m^{-2}, and the diurnal mean shortwave cloud forcing from -50 to -150 W m^{-2}. Previous studies have shown that in regions of deep convection, large clouds and rain cells express greater organization into structures composed of convective core regions attached to stratiform anvil cloud and precipitation. Entrainment of moist, cloudy air from the stratiform anvil into the convective core helps to sustain convection against the entrainment of unsaturated air. Thus large clouds produce more rain, trap more terrestrial radiation and reflect more solar energy than do smaller clouds. The combined effect of increased forcing and increased spatial coverage means that larger clouds contribute most of the total forcing. Rain cells larger than 10^5 km^2 make up less than 2% of the rain cell population, yet contribute greater than 70% of the latent heating. Similarly, the clouds larger than 10^5 km^2, in which the largest rain cells are embedded, make up less than 3% of clouds, yet are the source of greater than 90% of the total thermodynamic forcing. Significant differences are apparent between the scales of latent heating and radiative forcing, as only about 25% of cloud area is observed to precipitate. The fraction of clouds that contain some rain increases dramatically from about 5% for the smaller scale (10^3 km^2) to as high as 90% for the largest scale considered here (10^6 km^2). The fractional area of the precipitating cloud ranges from 0.2 to 0.4 with a hybrid scale dependence. Greater than half of radiative forcing is provided by nonprecipitating anvil portions of deep convective cloud systems. The results presented here have significant implications for the parameterization of clouds and rain in GCMs and washout of solute trace gases and aerosols in chemistry and transport models.

3.1 Introduction

In the tropical regions of deep convection, latent heating and cloud-radiative interactions play an important role in the energy balance. Large and frequent cloud systems deposit the majority of the total latent heating of the atmosphere in the Tropics. This heating provides the energy to lift parcels to the tropopause and balance longwave cooling of the atmosphere. Excess latent heating in these regions establishes zonal and meridional heating gradients in the atmosphere that play a crucial role in large-scale dynamics. Model studies and measurements of the radiative effects of convective-cirrus cloud systems at the top of the atmosphere and surface have confirmed that, in addition to latent heating, clouds: (a) reduce the flux of longwave radiation to space (the cloud greenhouse effect), resulting in heating concentrated mostly in the atmosphere; and (b) enhance the reflection of solar energy back to space, resulting in a cooling concentrated mostly at the surface (Ramanathan 1987; Collins et al. 1996). These radiative processes are responsible for enhancing the atmospheric heating gradient while simultaneously reducing the surface heating gradient between deep convective regions and regions of large-scale subsidence. This effect operates on zonal circulations, for example over the tropical Pacific Ocean (Webster 1994), as well as meridional circulations such as the Indian monsoon (Ramanathan 1987).

Tropical convective clouds span a continuous spectrum of sizes, from a few tens of km^2 to millions of km^2. Thus we can expect that the thermodynamic forcing of the column by clouds exists on a corresponding spectrum of sizes. Clouds of different sizes, however, express significant structural differences. Studies of satellite images (Roca and Ramanathan 2000) and ground-based radar echoes (Houze and Betts 1981) suggest that small clouds are dominated by isolated convective elements while larger clouds express an organized structure of one or more deep convective cores attached to a broad stratiform anvil cloud. Boer and Ramanathan (1997) document a significant dependence of solar reflectivity and outgoing longwave radiation on cloud size in the tropical western Pacific. Houze (1989) presented

observations of the vertical latent heating profiles of organized convective cloud systems, and demonstrated that they peak higher in the troposphere than profiles of isolated convective cells. Hartmann et al. (1984) show that applying the vertical heating profile consistent with organized cloud structures in an atmospheric general circulation model (GCM) results in a more realistic simulation of the Walker circulation than the simulated circulation when the heating profile consistent with isolated convective cells is applied. In order to understand the link between cloud thermodynamic forcing and atmospheric dynamics, we have to determine the spatial scales of the forcing.

The Tropical Rainfall Measuring Mission (TRMM) satellite provides, for the first time, simultaneous measurements of the latent heating and radiative forcing of clouds from the same platform. In this study, these measurements are used to investigate the dependence of thermodynamic forcing on the horizontal scales of tropical convective clouds over the Indian Ocean during the winter monsoon. Cloud thermodynamic forcing averaged over individual clouds and rain cells is evaluated in order to reveal the horizontal scales at which these processes force the large-scale atmospheric circulation of the Indian Ocean monsoon region. Furthermore, the horizontal scale and magnitude of latent heating is compared to that of radiative forcing for typical clouds across the observed spectrum of sizes. Finally, the analysis provides a convenient means of evaluating the parameterization of clouds and convection in GCMs. The horizontal scales of clouds and rain cells will be compared to typical grid box sizes in GCMs of various resolutions as a simple means of comparing the naturally occurring scales of thermodynamic forcing features to the minimum scales represented explicitly in models. Properly accounting for the effects of clouds large enough to be resolved by the model, while also capturing the effects of the subgrid-scale clouds, and subgrid-scale variability within clouds, through a parameterization scheme is a particular challenge in light of the continuous spectrum of clouds sizes. Satellite studies such as this can help constrain the problem of distinguishing between resolved forcing and subgrid-scale

forcing. Note that in this paper, the term "resolved" will be used to refer to clouds and rain cells whose size exceeds the size of a single grid box. That a cloud or rain cell is resolved by this definition does not mean that smaller-scale processes imbedded within the cloud or rain cell, which may be responsible for the growth and maintenance of the feature, will be resolved.

Data are presented from January and February 1998, during the winter monsoon season. The tropical Indian Ocean consists of a large pool of warm water with surface temperatures typically greater than 300 K. During the winter monsoon, convergence of northeasterly surface winds off of the Asian continent with southeasterly winds from the southern Indian Ocean over these warm waters results in frequent convective activity (Krishnamurti et al. 1997). The result is a large sample of convective clouds that provide an ideal environment for studying the thermodynamic forcing of tropical clouds.

3.2 TRMM data

TRMM is the first satellite specifically designed for the measurement of rainfall. The satellite is a joint US-Japan project that has a passive microwave radiometer, a passive visible and infrared radiometer, and the first ever spaceborne rain radar (Kummerow et al. 1998). Rainfall is measured independently from each of the instruments and algorithms are being developed that combine measurements from each of the instruments. In addition to the rainfall measuring instruments, the satellite also measures top of the atmosphere radiative fluxes with the Cloud and the Earth's Radiant Energy System (CERES) instrument (Wielicki et al. 1996). The choice of orbit parameters for TRMM was made with the goal of measuring the variability of tropical rainfall on time-scales from diurnal to annual (Simpson et al. 1988). It flies at a low orbit (about 350 km), which allows sufficient resolution to capture features of individual clouds of scales larger than a few hundred km^2. The orbit is inclined at 35° and precesses such that all local hours are sampled approximately once per month.

3.2.1 Passive microwave rain measurements

Surface rain rate estimates for this study were made at 5 km × 7 km resolution using the TRMM Microwave Imager (TMI), a 9-channel passive microwave radiometer. The instrument is nearly identical to the Special Sensor Microwave Imager (SSM/I), currently operating on polar-orbiting satellites, with an additional, dual-polarized low-frequency channel at 10.7 GHz (2.8 cm wavelength). Passive microwave rain measurements rely on both the emission and scattering properties of rain and ice at microwave frequencies. Furthermore, because the response function for each channel peaks at a different altitude within the atmosphere, the instrument can retrieve information about the vertical profile of rain and ice. The rain rate retrieval algorithm used in this study is described by Kummerow et al. (1996). It makes use of these properties to couple the observed brightness temperatures with a mesoscale cloud model. The technique uses a large database of candidate vertical profiles of hydrometeors and corresponding surface rain rates generated by the model. A forward calculation of the brightness temperatures that would be measured by the instrument if the actual hydrometeor profile matched that of the model profile is performed for each profile in the database. Under the assumption that profiles in the database occur with the same relative frequency as those in nature, the retrieved profile and rain rate comprises a weighted average of the model profiles and rain rates. The weighting of each model profile is determined from the difference between the measured properties and the modeled properties such as microwave brightness temperatures and the ratio of convective rain to stratiform rain. Random errors in this technique are roughly 100% and are associated with the spread of rain rates that might result in a given set of measured brightness temperatures. The algorithm was applied to SSM/I data and compared with ground-based radar by Olson et al. (1999). A positive bias error of about 20% is found to be associated with overestimates at low rain rates. These errors were found to decrease with spatial averaging. Furthermore, this error may be reduced with the improved resolution and additional channels of the

TMI. Estimates of vertically integrated latent heating are made directly from the surface rain rate retrievals using

$$\int (LH)dz = \rho_w L_v R_s$$

which states that the latent heating (LH) integrated through the depth of the cloud is equal to the density of water (ρ_w) times the latent heat of vaporization (L_v) and the surface rain rate (R_s).

3.2.2 Top of the atmosphere radiative flux measurements

Radiative flux measurements at the top of the atmosphere were made using the CERES instrument. CERES is modeled after the Earth Radiation Budget Experiment (ERBE) instruments that flew on the *ERBS*, *NOAA-9*, and *NOAA-10* satellites. While new algorithms are being developed to retrieve top of the atmosphere fluxes, initial processing of CERES data has been performed using the same algorithms as were applied to the ERBE data. These ERBE-like products are used in this study. The resolution of the CERES instrument is 10 km ✕ 10 km at nadir.

Cloud radiative forcing (CRF) is a simple and direct approach for estimating the effect of clouds on the radiative energy budget (Ramanathan 1987). CRF is the difference between the clear-sky radiative fluxes and the cloudy-sky fluxes, and thus reveals the radiative effects of clouds. Shortwave cloud forcing (C_s) is given by

$$C_s = S(\alpha_{clr} - \alpha),$$

where S is the incident solar flux, α_{clr} is the clear-sky albedo, and α is the cloudy albedo. Over oceans, the albedo of a cloud is almost always higher than the albedo of the surface. Therefore, C_s is usually negative and measures the cooling of the atmosphere-ocean column owing to the reduction in absorbed solar energy. Longwave cloud forcing (C_l) is given by

$$C_l = F_{clr} - F,$$

where F_{clr} is the clear-sky longwave flux to space and F is the cloudy longwave flux. Clouds are effective absorbers of longwave radiation and the upward flux of longwave energy above an overcast region is lower than if the region were clear. Thus C_l is positive and provides a measure of the increased longwave heating owing to the cloud. Typically, the cloudy-sky albedo and longwave flux values (α and F) are time- and space- averaged values. When CRF is calculated in this way, both the effects of the radiative properties of clouds as well as the effects of the frequency of cloud occurrence are accounted for. In this study, cloud forcing is averaged over regions that are entirely cloud covered. Thus α and F are the values for overcast skies. Cloud averaged CRF measurements used in this study represent the change in top of the atmosphere radiative flux at the location of the cloud from the clear-sky values owing to the presence of the cloud, and do not account for fractional cloud cover.

Clear-sky fluxes used in the cloud radiative forcing calculations are difficult to estimate on an instantaneous basis because of the high frequency of cloud cover. For this reason the monthly mean clear-sky longwave flux and albedo are used in place of the instantaneous clear-sky values. These are reported for 2.5° × 2.5° regions in the ERBE-like monthly mean product. To account for the variation of the clear-sky albedo with the solar zenith angle, only clear-sky albedo values measured at the same local hour as the pixel are used in calculating the monthly mean. To facilitate comparison of shortwave cloud forcing for clouds retrieved at different times of the day, and to account for presence of shortwave forcing only during daylight hours, all shortwave cloud forcing calculations are made using the diurnal mean solar insolation appropriate for the latitude of each cloud [calculated from Peixoto and Oort (1992), Eq. (6.18)].

The CERES radiometer measures radiances with an error of 1% or less. Additional uncertainty arises in converting the radiances measured from a single direction to top of the atmosphere fluxes resulting from radiation from all angles. For this conversion, an angular distribution model is used to estimate the anisotropy of the radiative flux. Reported errors

in instantaneous top of the atmosphere fluxes for the pixel-scale data are 12.1% in the shortwave and 5% in the longwave (Suttles et al. 1992; Wielicki et al. 1995). Monthly mean clear-sky fluxes have been used in place of instantaneous values. Natural variability in the tropical clear-sky albedo is 0.015, as reported by Conant et al. (1997). Variability in clear-sky longwave flux over the Indian Ocean for January, 1998 as measured by the CERES instrument is ± 5 W m^{-2}. For a typical clear-sky albedo of 0.08, these values correspond to an uncertainty of 7 W m^{-2} in C_s, hence -10 W m^{-2} is used as a threshold for detecting clouds. For typical cloudy conditions, uncertainties in CRF are ± 15 W m^{-2}.

3.2.3 Cloud and rain cell detection

Collocation of the rainfall and radiation datasets is achieved by binning each to the same 0.25° ✕ 0.25° grid. The data are compiled into ensembles of rain cells (where precipitation reaches the ground) and clouds (which may or may not contain precipitation). Rain cells are identified using a simple clustering technique whereby adjacent pixels of nonzero rain rate are grouped into a single cell. Although a different algorithm is used here, the clustering scheme is identical to that described in Mapes and Houze (1993). Precipitating pixels must share a side to be included in the same cell. Cloudy regions that are not raining are excluded from the population of rain cells. The population of clouds is found by identifying contiguous regions that reflect greater than 10 W m^{-2} of diurnal mean solar energy over average clear-sky conditions. The same clustering technique as used to identify the rain cells is applied to the C_s data to identify the clouds. The terms "rain cell" and "cloud" are often used in the literature with various definitions. These terms will be used throughout this paper to refer specifically to the features identified using the thresholds and clustering technique described above.

The boundaries for this study are $\pm 20^\circ$ latitude and 40° -120° longitude. The swath width of the TMI is about 760 km. Although the CERES swath is wider, the CERES data are restricted to those data points that fall within the TMI swath in order match the data
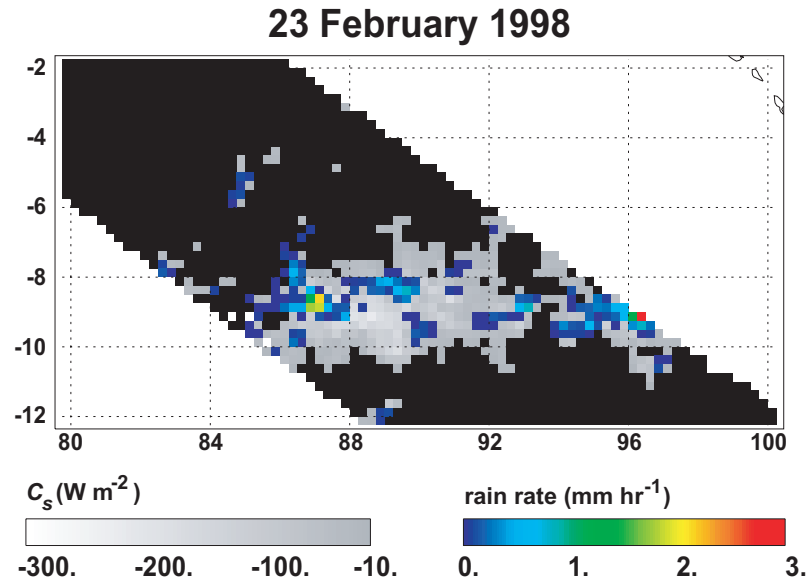
23 February 1998

Fig. 3.1. Clouds and rain cells detected by TRMM over the tropical Indian Ocean on 23 February 1998. Grid boxes where C_s is less than -10 W m^{-2} are shown in gray. Contiguous regions of such grid boxes are clustered into individual clouds. One large cloud is shown in the center of the swath with several smaller clouds surrounding it. Overlaid in color is surface rain rate. Contiguous regions of nonzero rain rate are clustered into rain cells. Rain cells always exist within a cloud. Several rain cells of varying size exist within the large cloud shown. Some of the surrounding clouds contain rain cells and others do not.

sets to the same grid. A land mask is applied and only 0.25° grid boxes lying entirely over ocean are included. Because shortwave reflectance properties are used to detect clouds, only satellite passes that occurred during daylight hours are used for the cloud statistics and the C_s statistics of rain cells. Furthermore, because at high solar zenith angles the incedent solar irradiance is low, which renders shortwave measurements highly uncertain at those times, only data acquired between 10 am and 3 p.m. (local time) are used for C_s measurements. Thus the full diurnal cycle of cloud amount is not accounted for in this study. All passes from all local hours are used for detecting rain cells. The CERES instrument is switched from a cross-track scanning pattern to a biaxial scanning pattern every third day. Data from the biaxial scan days is not dense enough to fill every 0.25° grid box at the edges of the swath. Thus no data was used from the biaxial scan days. Additionally, no CERES data was

available for Jan. 7 and 8. Thirty-eight days of data, for a total of 447 passes over the Indian Ocean region, are used in this study. Of these passes, 179 occurred in the middle of the day and were used for C_s measurements.

An example of the data for a pass over the Indian Ocean on 23 February 1998 is shown in Fig. 3.1. Here C_s is shown in gray-scale and surface rain rate is superimposed on color. A single large cloud appears in the center of the swath with several smaller clouds nearby. Within the large cloud are several rain cells of various sizes that are all attached to a large area of nonprecipitating anvil cloud. Some of the smaller clouds contain rain cells and others do not.

3.3 Spatial scales of clouds and precipitation

The horizontal scales of latent heating and CRF are revealed by the size distributions of rain cells and clouds. The numbers of rain cells and clouds detected in each size bin, from less than 10^3 km^2 to greater than 10^6 km^2, are shown in Fig. 3.2a (solid line and dotted line respectively). The lower and upper ranges of the scales are, respectively, limited by the resolution of the individual pixel and the swath width. The number of rain cells exceeds the number of clouds in most size bins because rain cells were detected using all passes of the satellite while clouds were detected using only midday passes. A total of 17,722 rain cells and 8707 clouds are included in the populations. Small cells and clouds dominate the populations with numbers decreasing steadily with size. The region greater than 5×10^5 km^2 is shaded in Fig. 3.2, and subsequent figures, to indicate that there is little confidence in the ability of the TRMM satellite to estimate rain cell and cloud size for those cells and clouds larger than 5×10^5 km^2. Because of the 760-km swath width, the sizes of clouds and cells in this region are likely to be underestimated. The placement of this gray region was tested against simulated clouds of a known size distribution by sampling the simulated clouds with the TRMM swath. The numbers of clouds were improperly sampled only within the gray region. The maximum sizes attainable for clouds and rain cells both fall within the gray region. Rain
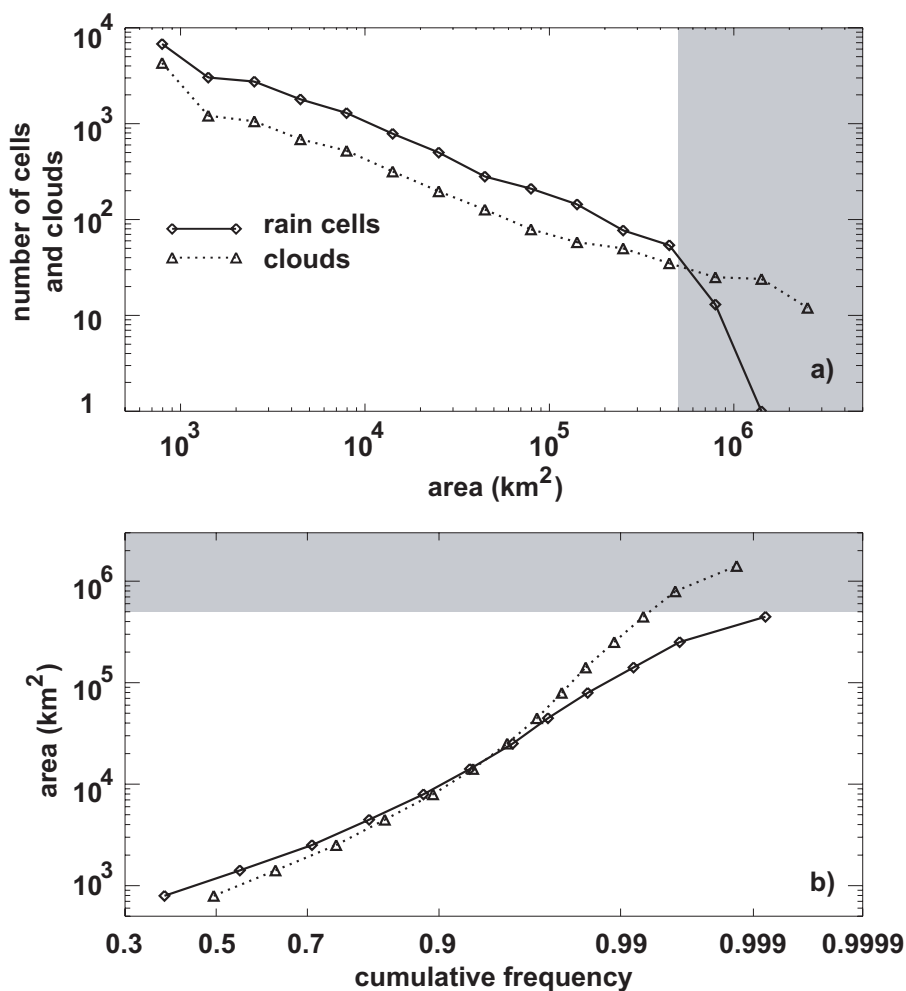
Fig. 3.2. (a) Number of rain cells (solid line) and clouds (dotted) as a function of area. (b) Cumulative frequency of occurrence of rain cells and clouds as a function of area. Cumulative frequency (abscissa) is shown on a normal probability scale.

cell number drops off rapidly at about 5×10^5 km². If rain cells in excess of 10^6 km² were to occur frequently, they would be truncated by the TRMM swath and would appear in the largest size bins in Fig. 3.2, as occurs in the distribution of clouds. However, only one rain cell larger than 10^6 km² is observed, indicating that the edge of the gray area in the figure corresponds roughly with the maximum rain cell size and confirms that the TRMM swath width is sufficient to capture most rain cells. On the other hand, geostationary satellite imagery confirms the presence of clouds in excess of 10^6 km² and even 10^7 km².

An alternative representation of the retrieved populations of rain cells and clouds for the 1998 winter monsoon are shown in Fig. 3.2b. The data are presented as the cumulative frequency of occurrence of rain cells and clouds on a log-probability plot. Plotted in this way, a straight line indicates that the data are lognormally distributed. The distribution of rain cells is approximately lognormal with deviations from lognormality at the small and large ends of the spectrum. The lognormal distribution of convective rain cells has been observed in radar echo studies conducted in tropical, midlatitude, oceanic, and continental convective regimes. Houze and Cheng (1977) and Lopez (1978), for example, demonstrate that in addition to radar echo size distributions, heights, and durations of radar echoes are also lognormally distributed. Deviations at the small and large extremes of the size range are likely due, in part, to limitation in the measurement resolution and observable swath width of the instrument, respectively. For rain cells, deviations at the large extreme may also be attributable to physical limitation of the rain cell growth process as mentioned above. Mapes and Houze (1993), for example, suggest 300 km as a limit for horizontal transport of precipitation-sized ice particles from the tops of convective cells before falling out, implying a low probability for rain cells exceeding 10^5 km^2.

Lognormal distributions are an outcome of processes exhibiting the law of proportionate effects (Aitchison and Brown 1957). This law states that as a variable progresses in steps, the amount the variable changes from its current value to the next value is a random proportion of its current value. That the law of proportionate effects may apply to the generation or growth processes of convective cells was discussed by Lopez (1977). In this paper it is proposed that either cell growth by merging of small convective elements or growth by scale-dependent entrainment may account for the lognormal distributions. An attempt to describe the behavior from first principles was provided by Raymond (1997), who suggests that mesoscale wind components as well as moisture flux components fit a lognormal distribution. Nevertheless, a complete explanation for the distributions remains

elusive.

The small clouds are distributed in a similar fashion as the rain cells. There is, however, a significant departure from the lognormal distribution appearing for clouds greater than 5×10^4 km^2, where large clouds appear more frequently than they would if the trend for the small clouds held for all clouds. Although we expect most of these clouds to be of convective origin, we would not necessarily expect that they adhere to the same distribution as the rain cells. Rain cells and small clouds are more directly related to convective-scale dynamics. The structure of the large cloud systems, however, can include a large anvil of cirrus cloud whose size may be more sensitive to larger-scale dynamics. Cirrus cloud may be advected by mean upper level winds or synoptic-scale divergence associated with large deep convective storms. A breaking scale is identified by Roca and Ramanathan (2000) in a satellite study of deep convective clouds over the Indian Ocean. For deep convective clouds greater than 10^4 km^2, greater organized structure is expressed in the form of deep convective core regions surrounded and connected by large stratiform anvil cloudiness. For clouds whose area exceeds the scale break, the fractional area of the cloud characterized by deep, undiluted convective activity increases with cloud size.

The likelihood that a cloud contains a precipitating region increases with size. The fraction of the number of clouds in each size bin that is observed to contain a rain cell is shown in Fig. 3.3 (solid line). Most observed clouds are not precipitating. Clouds smaller than 10^4 km^2 make up more than 85% of the cloud population, but only a small fraction of them contain any precipitation. For the subset of clouds that do contain some precipitation, the fraction of the cloud's area that is precipitating is shown in Fig. 3.3 (dashed line). Error bars in this and subsequent figures indicate one standard deviation of the mean in each size bin. Only 25-30% of the average cloud's area is raining. Clouds smaller than 2000 km^2 are too close to the resolution limit of the data to reliably estimate the raining fraction. For clouds from 2000 to 10^5 km^2 in size, the raining fraction of cloud decreases with
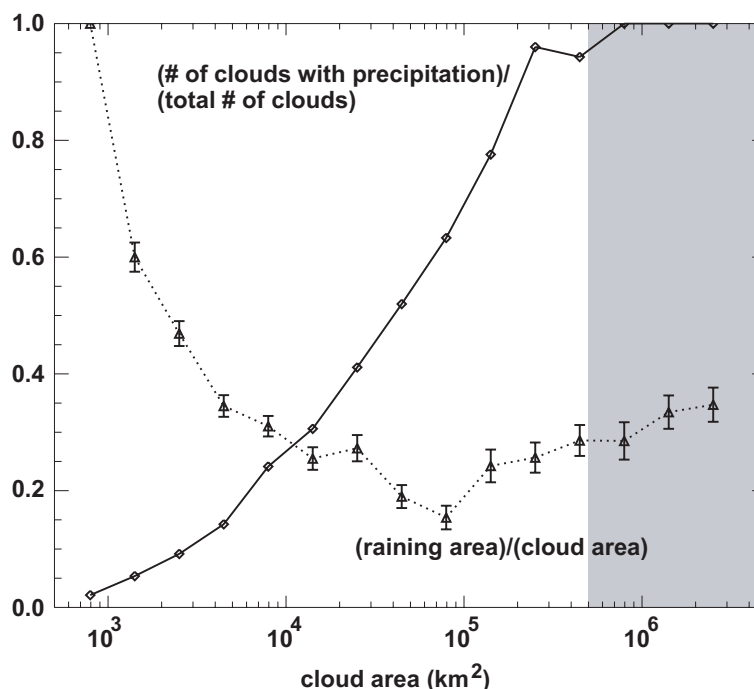
Fig. 3.3. Fraction of clouds that contain a rain cell (solid line). Also, the average fraction of cloud area taken up by rain cells (dotted), for clouds that contain at least one rain cell only. Both shown as a function of cloud area. Error bars indicate one standard deviation of the mean.

size, while for clouds larger than 10^5 km^2 raining fraction increases with size. The large clouds expressing an increasing scale dependence of raining fraction are the same clouds that deviate from the lognormal distribution as discussed above.

3.4 Thermodynamic forcing of rain cells

Embedded within some of the clouds lie the rain cells. Ground-based radar observations of rain cells made during the Global Atmospheric Research Program's Atlantic Tropical Experiment (GATE) confirmed that larger rain cells, termed mesoscale precipitating features (MPFs), express organized structure just as the large clouds do (Houze and Betts 1981). One or more deep convective core regions are connected to a broad region of stratiform precipitation in MPFs. The rain rate within the core is large and associated with vigorous updrafts. Precipitation within the stratiform region comprises ice detrained from the upper portion of the convective cell and is associated with much weaker, but more broadly
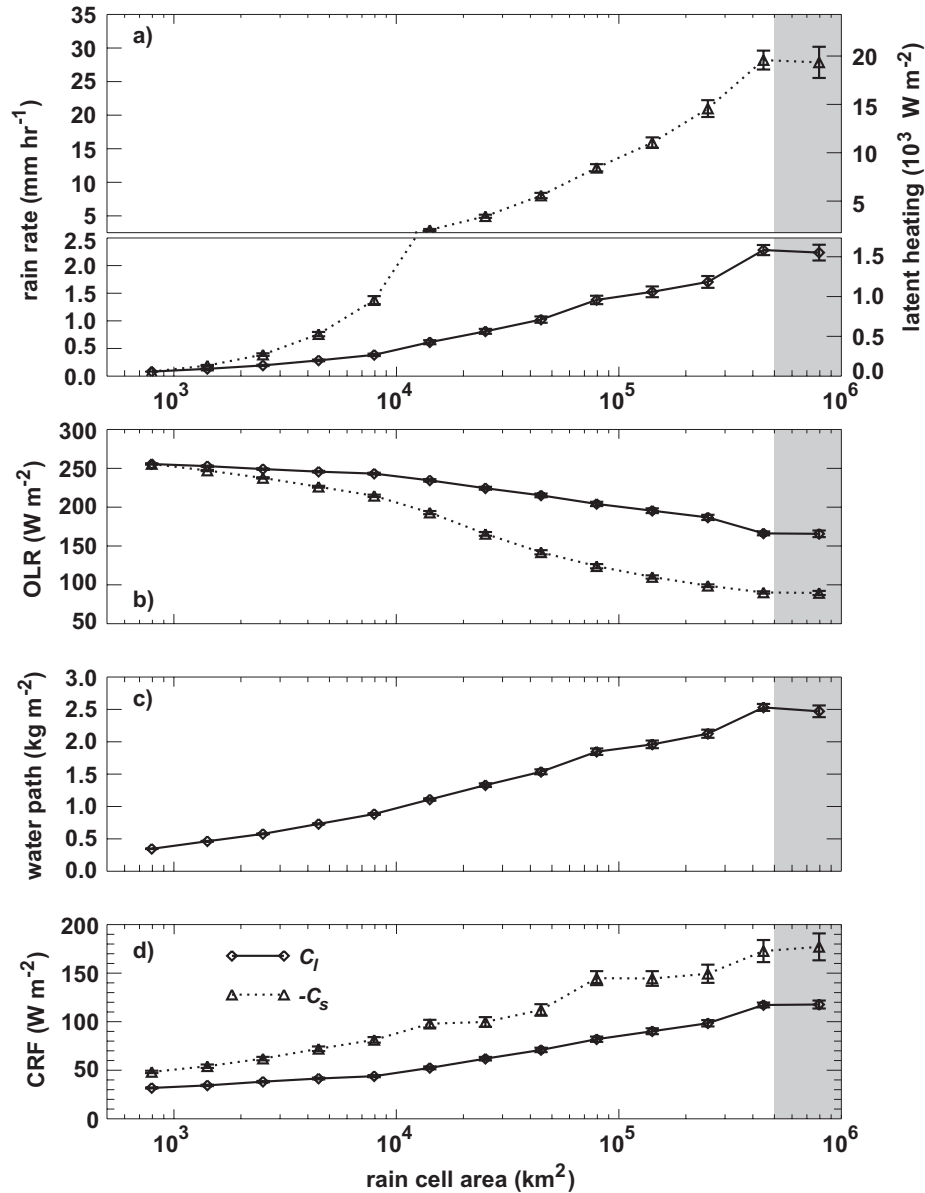
Fig. 3.4. Rain cell averaged properties as a function of rain cell area. (a) Rain rate (solid line) and 0.25° peak rain rate (dotted). Right side axis scaled to show vertically integrated latent heating. (b) OLR (solid) and 0.25° minimum OLR (dotted). (c) Ice+liquid water path. (d) C_l (solid) and $-C_s$ (dotted). Error bars indicate one standard deviation of the mean.

distributed, mesoscale motions. The organization of the larger precipitating clouds into a mesoscale convective/stratiform structure appears to be associated with more intense convective activity. The resolution of TRMM data is probably not sufficient to capture individual convective showers, but the scales of the rain cells detected here provide an

indication of the scales at which the convective and stratiform showers organize themselves into the MPF structure. By using satellite measurements of rainfall, rain cells up to an order of magnitude larger than those measured during GATE are detected.

Rain cell properties as a function of rain cell size are shown in Fig. 3.4. Cell-averaged rain rate increases with rain cell size (Fig. 3.4a). Average latent heating of rain cells is proportional to the surface rain rate. The axis on the right side of Fig. 3.4a has been scaled to indicate the average vertically integrated latent heating from the retrieved rain rate. Latent heating increases with rain cell size, the largest cells releasing in excess of 1500 W m^{-2}. To indicate activity in the core of the MPFs, the size dependence of the rain rate in the 0.25° grid box where rain is heaviest is also shown in Fig. 3.4a (dashed line). Convective core rain rate increases rapidly with size, particularly for the larger rain cells. Lopez (1978) hypothesized rain cells exhibiting an organized MPF structure are protected from entrainment of dry environmental air by the surrounding moist environment of the stratiform anvil cloud, generating more rain and creating taller clouds (Houze and Cheng 1977).

Dense cumulonimbus clouds emit longwave radiation from just the top portion of the cloud, thus average outgoing longwave radiation (OLR, solid line in Fig. 3.4b) is an effective indicator of cloud-top height. OLR decreases with the size of the rain cells suggesting that, on average, larger rain cells penetrate to higher (colder) altitudes. The dotted curve in Fig. 3.4b is the scale dependence of OLR in the core area of the cell and indicates that the maximum height reached by a rain cell increases with size. The tops of the largest convective cores can penetrate to the tropopause.

Similarly, the vertically integrated liquid + ice water path increases with cell size (Fig. 3.4c). Apparently, larger convective cells are more effective at gathering moisture and distributing it vertically in the column. Were convective cells to grow primarily through the merger of small convective elements, there would be no appreciable source of additional moisture. Mesoscale motions within MPFs must directly enhance the convergence of

moisture below the cloud or act to concentrate the moisture captured from each element.

Longwave radiative forcing of a cloud measures the reduction in OLR attributable to the presence of the cloud. This effect increases with the horizontal scale of rain cells (Fig. 3.4d, solid line). Ramanathan (1977) demonstrated that the longwave forcing effect of a cloud is largely dependent on the difference between the surface temperature and the cloud-top temperature. The observed increase in cloud greenhouse effect with size is a result of the increase in cloud-top height with size discussed above.

Consistent with the deeper cloudiness indicated by the decreasing OLR and increasing water+ice path, the albedo, and thus shortwave cloud forcing, increases with rain cell size for nearly all size bins (Fig. 3.4d, dashed line). This indicates that the larger rain cells cool the column more effectively than the smaller rain cells.

3.5 Thermodynamic forcing of clouds

Figure 3.4 indicates that rain-cell-averaged latent heating exceeds rain-cell-averaged CRF by as much as one order of magnitude. Recall, however, that only 25% of cloud area is precipitating. The remaining three quarters of cloud area comprises nonprecipitating portions of extended anvil cloud associated with deep convective systems, dissipating deep convective clouds, and nonprecipitating shallow cumulous. Although this portion of the cloud area contributes no latent heating, it has significant shortwave and longwave radiative effects.

Deep convective clouds dominate the population of the larger winter monsoon clouds over the Indian Ocean (Roca and Ramanathan 2000) and give rise to extended decks of anvil cloud through detrainment of ice near the top of the cloud. Indeed, Webster and Stephens (1980) observed the ubiquitous presence of middle and high clouds, sometimes extending 750 km from the center of convection, over the South China Sea during the winter monsoon. Ramanathan and Collins (1991) suggested that the C_s of large decks
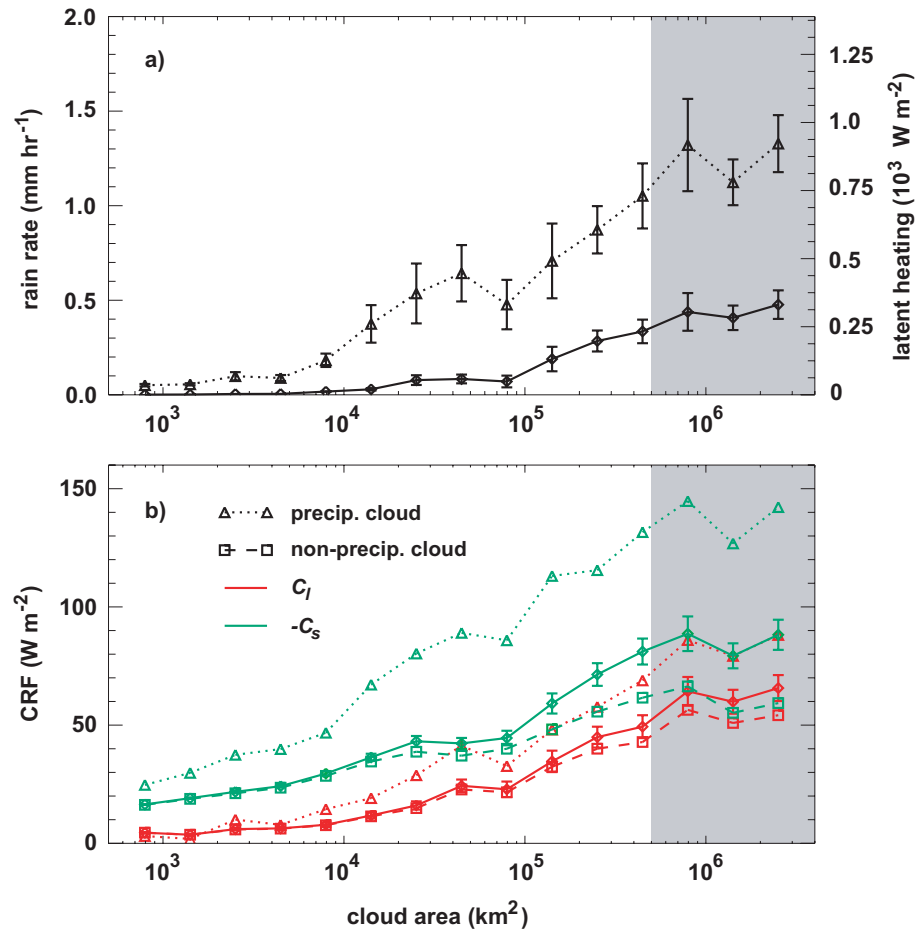
Fig. 3.5. Cloud averaged properties as a function of cloud area. (a) Rain rate; right side axis scaled to show vertically integrated latent heating. (b) C_l (red) and $-C_s$ (green). Solid lines are averages over entire cloud, dotted lines are averages over precipitating portions of cloud, and dashed lines are averages over non-precipitating portions of cloud. Error bars indicate one standard deviation of the mean.

of anvil cloud may strongly influence heating of the ocean surface in the western Pacific warm pool.

Latent heating as a function of cloud size is shown in Fig. 3.5a. The solid line denotes the latent heating averaged over the entire area of the cloud, and the dotted line is latent heating averaged over only the portion of cloud that contains rain. Latent heating increases with cloud size. For clouds larger than 10^5 km^2, the slope of the increase is more dramatic. Evidently, the larger, more organized clouds contain within them the larger rain

cells, which were found to be the dominant source of rainfall.

Similar to the results from the rain cells, cloud-averaged OLR decreases and albedo increases with cloud size (not shown). The corresponding dependence of CRF on cloud size is shown in Fig. 3.5b. Here C_l is shown in red and C_s in green. The dashed lines indicate averages over the nonprecipitating portions of cloud, the dotted lines are averages over the precipitating portions of cloud, and the solid lines are average over the entire cloud area. The distinction between precipitating cloud and nonprecipitating cloud is made based on the surface rain rate. Cloudiness that contains precipitation that reevaporates before striking the ground, which results in no net latent heating, is considered nonprecipitating. The goal here is to compare radiative forcing in cloudiness that contributes to net latent heating to cloudiness that does not. For small clouds, the average CRF for the nonprecipitating cloud is roughly equal to the total cloud-averaged CRF, since most of the small clouds do not contain any precipitation. For all cloud sizes, however, precipitating cloud averaged CRF exceeds nonprecipitating cloud CRF. This difference increases with cloud size. Also note that the C_s difference between precipitating cloud and nonprecipitating cloud is greater than that for C_l in the large clouds. Cells of active convection apparently generate thicker and more reflective clouds locally in the precipitating region. Although the extended anvil cloud is comprised of ice detrained at the top of the convective core, the material that remains aloft to produce the nonprecipitating cloud is less densely concentrated and distributed over a thinner vertical layer. Thus it is less effective at reflecting sunlight and trapping longwave energy. Note, however, that the magnitudes of CRF in the nonprecipitating regions are quite significant, exceeding 60 W m^{-2} in the largest clouds. The albedo of cirrus clouds is associated with its optical depth, which can depend on physical thickness of the cloud as well as the amount, size, and shape of ice crystals at the top of the cloud. Observations suggest, however, that albedo may be more sensitive to cloud thickness than microphysics (Heymsfield et al. 1998). Cloud-averaged latent heating exceeds cloud-averaged CRF by about a factor of 3 or 4 for

the large, deep convective clouds.

3.6 GCM parameterization of clouds and convection

Evaluating the properties of clouds as a function of their size provides a useful tool for evaluating the treatment of clouds in GCMs. The horizontal grid scales of many such models are within the horizontal scale of the larger clouds detected using the TRMM satellite. Using the definition stated in the introduction of the paper, these clouds are resolved by some models. While the aggregate effect of unresolved clouds and subgrid-scale processes within resolved clouds on the state of the surface-atmosphere column in each grid box must be determined using a parameterization scheme, some of the effects of resolved clouds may be determined explicitly and separate from the parameterization. Since clouds exist on all scales, from entirely subgrid-scale to fully resolved, separating the effects of clouds into resolved and unresolved forcing, while still capturing the proper scale dependence of forcing across the spectrum of cloud sizes, poses a particular challenge to modeling efforts.

The cumulative contribution of rain cells and clouds to the total thermodynamic forcing is shown in Fig. 3.6 as a function of the rain cell and the cloud size. The vertical dashed lines indicate typical values for the horizontal resolution of spectral GCMs at the equator. The enhanced forcing of larger rain cells, in conjunction with their larger spatial extent, mean that a relatively small number of large rain cells account for a large fraction of the total observed latent heating and CRF attributable to the rain cells (Fig. 3.6a). Rain cells greater than 10^5 km^2 make up less than 2% of all cells, yet contribute roughly 70% of latent heating.

Presented in this way, the data indicates the fraction of thermodynamic forcing contributed by rain cells that are resolved by the model and the fraction resulting from unresolved cells. Note however that, although the total dimension of a rain cell may be larger than the GCM resolution (*i.e.*, resolvable), there will be individual rain features that
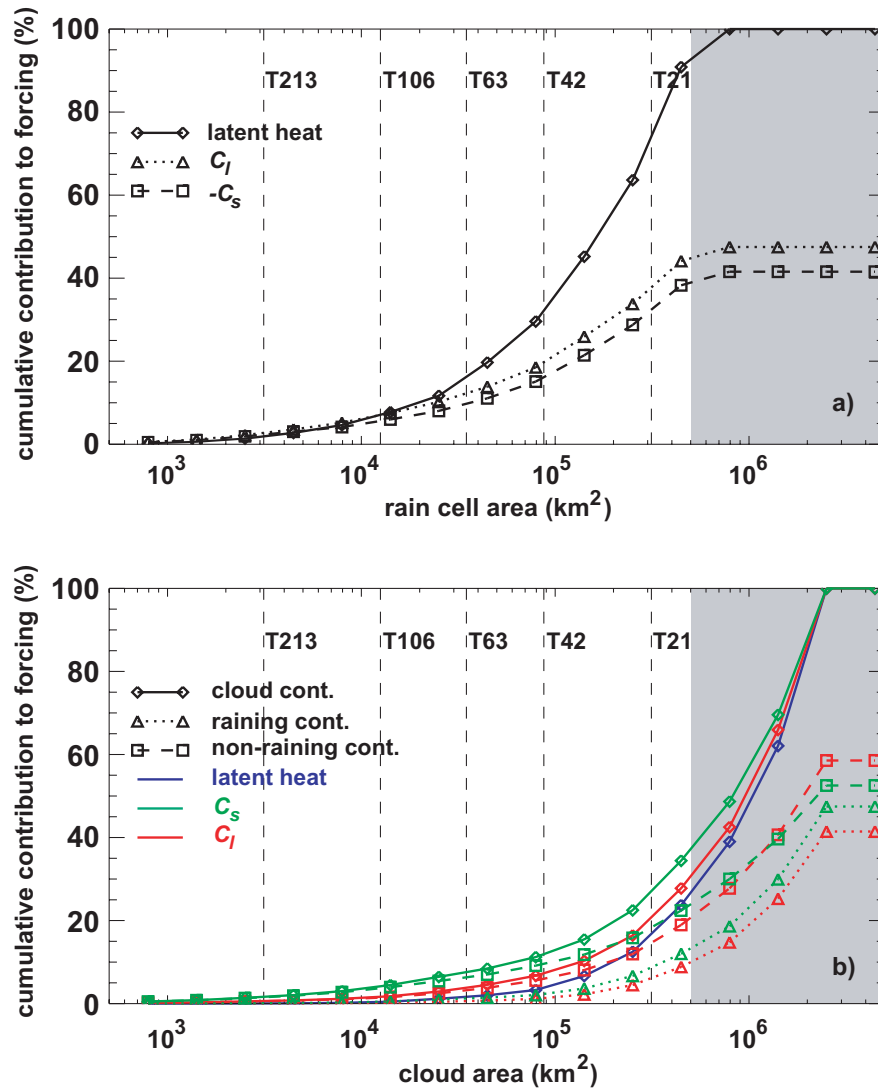
Fig. 3.6. (a) Cumulative contribution of rain cells to total latent heating (solid), C_l (dashed line) and C_s (dotted) as a function of rain cell area. (b) Same for clouds. Blue is latent heating, green is C_s and red is C_l. Solid lines are the contributions from the entire cloud, dotted lines are the contributions from the precipitating portions of cloud and dashed lines are the contributions from non-precipitating portions of cloud.

are subgrid-scale that need to be parameterized, even if the whole rain cell is resolvable.

The amount of latent heat and CRF attributable to resolved rain cells is a strong function

of model resolution. A GCM with the highest resolution, T213 (approx. 50 km $\times$ 50 km),

would resolve enough of the rain cells to account for virtually all of the rain cell forcing.

By resolving these rain cells, it is possible to identify such features in the model and test

the resolved physics, as well as the parameterizations of subgrid-scale processes, to see if they result in resolved rain cells that have scale dependent properties that are consistent with observed rain cells. Latent heating and CRF of monsoon rain cells in such a model should express a similar size dependence as shown in Fig. 3.4. A GCM at the lowest resolution (T21 = approx. 550 km × 550 km), however, would only resolve enough rain cells to account for about 30% of rain cell forcing.

As is the case with rain cells, the largest clouds contribute most of the thermodynamic forcing (Fig. 3.6b). Clouds larger than 10^5 km^2 contribute more than 80% of the latent heating (blue line), C_l (red lines), and C_s (green lines). The solid lines are the cumulative contribution of the entire area of the clouds in each size bin to the total cloud forcing. The dotted and dashed lines are the contributions of the precipitating area of cloud and the nonprecipitating area of cloud, respectively, to the total forcing. Note that the nonprecipitating cloud is a significant contributor to total CRF. While latent heating dominates CRF in rain cells, the nonprecipitating cloud, because of its spatial extent, contributes more than half of the total observed CRF.

That the largest clouds provide such a large contribution to total forcing is important, because even coarse-resolution GCMs should, in principle at least, resolve many of these large clouds. As with the resolved rain cells, care must be taken as GCMs will still need parameterizations for some subgrid-scale features to properly simulate these large clouds. Even at the coarsest model resolution, clouds contributing greater than 80% of the observed latent heating are resolved. The rain cells in these clouds may not be resolved, as discussed above, but this result indicates that the large clouds contain several rain cells and that these are the larger rain cells that are contributing most of the latent heat. CRF, however, is a process that scales with the size of the entire cloud. A GCM at T21 resolution will resolve clouds contributing greater than 75% of CRF. At a resolution of T63 (approx. 200 km × 200 km) enough clouds are resolved to account for greater than 90% of CRF.

Comparison of the scale dependence of cloud frequency and CRF in GCMs to the trends detected by TRMM provides a means of validating of the treatment of clouds in GCMs. The dependence of rainfall, cloud liquid water path, and other properties on cloud size for resolved tropical Pacific clouds in a GCM is demonstrated in Zhang et al. (1999). They also compare modeled cloud distributions to distributions observed by the GMS satellite to identify strengths and weaknesses in the model's cloud parameterization scheme.

The cumulative contributions to the thermodynamic forcing of clouds and rain cells (Fig. 3.6) indicate that larger clouds and rain cells, known to be associated with organized convection (Roca and Ramanathan 2000), are the dominant source of forcing. However, we still need to understand how individual convective elements, with scales of tens of kilometers, organize themselves to give rise to the large-scale forcing. GCMs have to deal with this subgrid-scale problem rigorously for simulating the observed importance of the "resolved"-scale clouds.

3.7 Discussion and conclusion

Thermodynamic forcing of the ocean-atmosphere column by clouds is provided by latent heating and cloud-radiative interactions. Measurements from the TRMM satellite of surface rain rate and top of the atmosphere radiative fluxes provide estimates of the total thermodynamic forcing of winter monsoon clouds over the Indian Ocean. The total latent heating averaged over all January and February 1998 passes over the Indian Ocean (including clear-sky regions) is 118 W m^{-2}. For C_l, the average is 22 W m^{-2} and average C_s is -32 W m^{-2}. Assembling the data into populations of rain cells and clouds highlights the horizontal scales at which the latent heating and CRF processes operate, and allow for the comparison of the magnitudes of latent heating and CRF on the scales of individual clouds.

Thermodynamic forcing increases with size for both the rain cells and the clouds. The combined effects of increased coverage and increased thermodynamic forcing exhibited by the larger clouds in the study, implies an important role for large clouds in the overall

heating and cooling of the column. Less than 2% of rain cells are found to contribute roughly 70% of the total latent heating. All of these cells are between 10^5 and 10^6 km². In 447 passes over the Indian Ocean during the two months of observations, this amounted to only 499 rain cells, or roughly one cell at the dominant scale for each pass. Riehl and Malkus (1958) concluded that a relatively few deep convective towers (1500-5000 throughout the equatorial region from 10ºN to 10ºS) carry enough heat to the upper troposphere to balance the radiative cooling and poleward transport in the upper branch of the Hadley circulation. Rain cells are not directly comparable to the deep convective towers addressed by Riehl and Malkus because several such towers may exist within a single rain cell. Riehl and Malkus proposed that the towers representing the core regions of undiluted, penetrative convection are 3 to 5 km on a side – numbers that were confirmed by observations during GATE (LeMone and Zipser 1980). While the deep, undiluted towers are critical for transporting heat from the boundary layer to the tropopause, the emphasis in the present study is on the scales forcing the large-scale features of the tropical monsoon circulation. Consideration of the towers alone ignores the important contribution to forcing from the stratiform anvil precipitation. Mapes and Houze (1995) demonstrate that the large-scale environment in which the deep convective clouds are embedded respond to heating from both stratiform precipitation and convective precipitation, and hence the entire rain cell. A complementary calculation to that of Riehl and Malkus can now be made to determine how many rain cells at the dominant scale are required at a given time to provide the 118 W m^{-2} latent heating of the winter monsoon. Taking 2×10^5 km² as a representative size for a deep convective rain cell, with an area averaged latent heating of 1000 W m^{-2}, and 4×10^7 km² as the area of the tropical Indian Ocean, it takes only about 20 rain cells at a time to provide the necessary latent heat.

Only 25-30% of a typical monsoon cloud is raining. In contrast to the latent heating, which is confined just to the rain cells within a cloud, CRF is distributed throughout the

entire area of the cloud system. The dominant scale of the clouds is at least one order of magnitude larger than that of the rain cells. Clouds greater than 10^5 km^2, comprising less than 3% of all observed clouds, are found to contribute 90% of the total CRF. Indeed, many of these clouds are beyond the size range that the TRMM swath can capture. Although operating at different scales, latent heating and CRF remain linked since the same clouds that provide most of the CRF also provide most of the latent heat. Evidently, the largest rain cells are embedded only within the largest clouds.

Increasing thermodynamic forcing with cloud size is likely a reflection of the dominance of organized deep convection at larger cloud sizes in the tropical Indian Ocean. One or more large precipitating regions in the core of the cloud system are associated with vigorous convective motions penetrating to the tropopause. Within these precipitating regions, latent heating exceeds CRF by one order of magnitude. Large amounts of ice are detrained from the tops of the convective cores and mesoscale circulations effectively disperse the anvil material. The number distribution of these giant organized cloud systems reveals a separate regime from the smaller scale, lognormally distributed rain cells, and shallow cumulus.

The nonprecipitating cloud contributes no latent heating, yet has significant radiative properties and, because of its spatial extent, contributes more than half of the total CRF. Within a rain cell, atmospheric latent heating can exceed top of the atmosphere CRF by up to a factor of 10. Averaged over the entire area of a deep convective cloud system, however, latent heating exceeds CRF by only a factor of 3 or 4. The magnitude of CRF increases with cloud size. Cooling owing to C_s exceeds the warming from C_l at all size bins such that the largest clouds detectable by TRMM provide a net cooling of the column of about 30 W m^{-2}. In addressing the response of the large-scale circulation to the thermodynamic forcing, it is important to consider the vertical distribution of the forcing. Table 3.1 shows the partitioning of each component of the thermodynamic forcing for the average overcast

Table 3.1. Vertical distribution of the thermodynamic forcing for an average cloud (W m^{-2}).

	Latent heat[*]	C_s	C_l
Top of atmosphere	0	-70	48
Atmosphere	216	18	41
Surface[**]	0	-88	7

[*] Latent heat contained within 25% of the average cloud's total area.
[**] Surface CRF estimated from ratios of surface forcing to TOA forcing observed over the Central Equatorial Pacific Ocean during CEPEX (Collins et al. 1996).

region between the top of the atmosphere, the atmosphere and the surface. These values differ from those discussed at the beginning of this section because the clear-sky regions are excluded here. Also recall that cloud-averaged forcing is only determined from midday passes of the satellite, so these values are subject to large uncertainties due to poor sampling of the diurnal cycle of clouds and rain cells. Latent heating occurs entirely within the atmospheric layer, providing additional buoyancy and allowing clouds to penetrate deeper. CRF is observed by satellite at the top of the atmosphere. This is a forcing of the entire ocean-atmosphere column and hence is the sum of CRF in the atmosphere and at the ocean surface. While net cooling due to CRF is smaller than the magnitudes of either C_l or C_s, partitioning of each between the surface and atmosphere is different, and care must be taken in interpreting the cancellation of C_l and C_s. Observations of CRF at the surface and top of the atmosphere were made for deep convective clouds during the Central Equatorial Pacific Experiment (CEPEX) by Collins et al. (1996). The ratio of C_s at the surface to C_s at the top of the atmosphere was estimated to be between 1 and 1.5 indicating that in the absence of solar absorption in clouds, all of the cooling is felt at the surface. If moderate solar absorption occurs, then surface cooling is even larger to balance the atmospheric heating. The net result in either case is to stabilize the entire column. Taking an intermediate value of 1.25 for this ratio leads to a cloud average cooling of the surface of -88 W m^{-2} and a moderate heating of the atmosphere of 18 W m^{-2} from absorbed sunlight. Here C_s in the atmosphere may have a limited impact on the direct response of the atmosphere to the

cloud in light of the large atmospheric latent heating. The strong surface cooling, however, has a significant effect on the tropical circulation on longer timescales (*e.g.*, Ramanathan and Collins 1991). In contrast, the ratio of surface C_l to top of the atmosphere C_l was estimated at between 0 and 0.3, meaning that surface heating due to longwave cloud radiation is small. Here C_l is expressed as a large convergence of upward longwave flux in the cloud that reinforces the latent heating by further destabilizing the cloud layer. Adopting an intermediate ratio of 0.15, cloud-averaged C_l in the atmosphere is 41 W m^{-2} leaving only 7 W m^{-2} to heat the surface. Values for surface and atmosphere radiative forcing are highly uncertain ($\pm$50%). In situ measurements of surface forcing are required to confirm these values for monsoon clouds.

Satellite measurements of the cumulative contributions of clouds to thermodynamic forcing provide a means of comparing the net effects of clouds resolvable by GCMs to subgrid-scale clouds. Clouds contributing the majority of thermodynamic forcing occur at scales larger than a grid cell in many models. Measurements of the scale dependence of cloud properties can be compared with those of modeled clouds to validate the treatment of resolved clouds in GCMs. The dominance of such large clouds in the thermodynamic forcing of the atmosphere in the tropical monsoon environment underscores the importance of the processes that organize convection in large-scale disturbances and their representation in models.

References

Aitchison, J. and J. A. C. Brown, 1957: *The Lognormal Distribution*. Cambridge University Press, 176 pp.

Boer, E. R. and V. Ramanathan, 1997: Lagrangian Approach for Deriving Cloud Characteristics from Satellite Observations and its Implications to Cloud Parameterization. *J. Geophys. Res.,* **102**, 21,383-21,399.

Collins, W. D., F. P. J. Valero, P. J. Flatau, D. Lubin, H. Grassl and P. Pilewskie, 1996: Radiative Effects of Convection in the Tropical Pacific. *J. Geophys. Res.,* **101**, 14,999-15,012.

Conant, W. C., V. Ramanathan, F. P. J. Valero, J. Meywerk, 1997: An Examination of the Clear-Sky Solar Absorption over the Central Equatorial Pacific: Observations versus Models. *J. Climate,* **10**, 1874-1884.

Hartmann, D. L., H. H. Hendon, and R. A. Houze, 1984: Some Implications of the Mesoscale Circulation in Tropical Cloud Clusters for Large-Scale Dynamics and Climate. *J. Atmos. Sci.,* **41**, 113-121.

Heymsfield, A. J., G. M. McFarquhar, W. D. Collins, J. A. Goldstein, F. P. J. Valero, J. Spinhirne, W. Hart and P. Pilewski, 1998: Cloud Properties Leading to Highly Reflective Tropical Cirrus: Interpretations from CEPEX, TOGA COARE, and Kwajalein, Marshall Islands. *J. Geophys. Res.,* **103**, 8805-8812.

Houze, R. A., 1989: Observed Structure of Mesoscale Convective Systems and Implications for Large-Scale Heating. *Q. J. R. Meteorol. Soc.*, **115**, 425-461.

Houze, R. A., and C.-P. Cheng, 1977: Radar Characteristics of Tropical Convection Observed During GATE: Mean Properties and Trends Over the Summer Season. *Mon. Wea. Rev.,* **105**, 964-980.

Houze, R. A., and A. K. Betts, 1981: Convection in GATE. *Rev. Geophys. Space Phys.,* **19**, 541-576.

Krishnamurti, T. N., B. Jha, P. J. Rasch and V. Ramanathan, 1997: A High Resolution Global Reanalysis Highlighting the Winter Monsoon. Part 1, Reanalysis Fields. *Meteorol. Atmos. Phys.,* **64**, 123-150.

Kummerow, C., W. S. Olson and L. Giglio, 1996: A Simplified Scheme for Obtaining Precipitation and Vertical Hydrometeor Profiles from Passive Microwave Sensors. *IEEE Trans. Geosci. Remote Sensing,* **34**, 1213-1232.

Kummerow, C., W. Barnes, T. Kozu, J. Shiue and J. Simpson, 1998: The Tropical Rainfall Measuring Mission (TRMM) Sensor Package. *J. Atmos. Ocean Technol.,* **15**, 809-817.

LeMone, M. A. and E. J. Zipser, 1980: Cumulonimbus Vertical Velocity Events in GATE. Part I: Diameter, Intensity and Mass Flux. *J. Atmos. Sci.*, **37**, 2444-2457.

Lopez, R. E., 1977: The Lognormal Distribution and Cumulus Cloud Populations. *Mon. Wea. Rev.*, **105**, 865-872.

Lopez, R. E., 1978: Internal Structure and Development Processes of C-Scale Aggregates of Cumulous Clouds. *Mon. Wea. Rev.,* **106**, 1488-1494.

Mapes, B. E. and R. A. Houze, 1993: Cloud Clusters and Superclusters over the Oceanic Warm Pool. *Mon. Wea. Rev.,* **121**, 1398-1415.

Mapes, B. E. and R. A. Houze, 1995: Diabatic Divergence Profiles in Western Pacific Mesoscale Convective Systems. *J. Atmos. Sci.*, **52**, 1807-1828.

Olson, W. S., C. D. Kummerow, Y. Hong and W.-K. Tao, 1999: Atmospheric Latent Heating Distributions in the Tropics Derived from Satellite Passive Microwave Radiometer Measurements. *J. Appl. Met.,* **38**, 633-664.

Peixoto, J. P. and A. H. Oort, 1992: *Physics of Climate.* American Institute of Physics, 520 pp.

Ramanathan, V., 1977: Interactions between Ice-Albedo, Lapse-Rate and Cloud-Top Feedbacks: An Analysis of the Nonlinear Response of a GCM Climate Model. *J. Atmos. Sci.,* **34**, 1885-1897.

Ramanathan, V., 1987: The Role of Earth Radiation Budget Studies in Climate and General Circulation Research. *J. Geophys. Res.,* **92**, 4075-4095.

Ramanathan, V. and W. D. Collins, 1991: Thermodynamic Regulation of Ocean Warming by Cirrus Clouds Deduced from Observations of the 1987 El Niño. *Nature,* **351**, 27-32.

Raymond, W. H., 1997: A Theoretical Evaluation of the Relevance of Lognormal Distributions for the Moisture Flux and Wind Components. *Mon. Wea. Rev.*, **125**, 3018-3023.

Riehl, H. and J. S. Malkus, 1958: On the Heat Balance in the Equatorial Trough Zone. *Geophysica,* **6**, 503-538.

Roca, R. and V. Ramanathan, 2000: Scale Dependence of Monsoonal Convective Systems over the Indian Ocean. *J. Climate,* **13**, 1286-1289.

Simpson, J., R. F. Adler, and G. R. North, 1988: A proposed Tropical Rainfall Measuring Mission (TRMM) Satellite. *Bull. Amer. Meteor. Soc.,* **69**, 278-295.

Suttles, J. T., B. A. Wielicki, and S. Vemury, 1992: Top-of-Atmosphere Radiative Fluxes: Validation of ERBE Scanner Inversion Algorithm Using *Nimbus-7* ERB Data. *Bull. Amer. Meteor. Soc.,* **31**, 784-796.

Webster, P. J., 1994: The Role of Hydrological Processes in Ocean-Atmosphere Interactions. *Rev. Geophys.* **32**, 427-476.

Webster, P. J. and G. L. Stephens, 1980: Tropical Upper-Tropospheric Extended Clouds: Inferences from Winter MONEX. *J. Atmos. Sci.,* **37**, 1521-1541.

Wielicki, B. A., R. D. Cess, M. D. King, D. A. Randall and E. F. Harrison, 1995: Mission to Planet Earth: Role of Clouds and Radiation in Climate. *Bull. Amer. Meteor. Soc.,* **76**, 2125-2153.

Wielicki, B. A., B. R. Barkstrom, E. F. Harrison, R. B. Lee, G. L. Smith and J. E. Cooper, 1996: Clouds and the Earth's Radiant Energy System (CERES): An Earth Observing System Experiment. *Bull. Amer. Meteor. Soc.,* **77**, 853-868.

Zhang, G. J., D. Zurovac-Jevtic and E. R. Boer, 1999: Spatial Characteristics of the Tropical Cloud Systems: Comparison Between Model Simulation and Satellite Observations. *Tellus*, **51A**, 922-936.